frontiers in Materials

ORIGINAL RESEARCH
published: 13 September 2021
doi: 10.3389/fmats.2021.652614

Experimental Study on the Piezoresistivity of Concrete Containing Steel Fibers, Carbon Black, and Graphene

Shijun Wang[1], *Amardeep Singh*[2] *and Qiong Liu*[3]*

[1]Economic and Technical Research Institute of Gansu Electric Power Corp., Lanzhou, China, [2]College of Civil Engineering, Tongji University, Shanghai, China, [3]School of Environment and Architecture, University of Shanghai for Science and Technology, Shanghai, China

Adding conductive materials to cement-based composites can lead to pressure-sensitive properties. In this study, different scales of conductive materials were incorporated, including macro-scale steel fibers, micro-scale carbon black powder, and nano-scale graphene. The coupling effect of three scales of materials ensured that the intelligent concrete had improved strength, lower cost, and comparable pressure-sensitive performance. The results show that the strength of intelligent concrete with multi-scale conductive materials is higher than that of the contrast group of ordinary concrete and intelligent concrete when adding nano-scale graphene alone. Especially, the addition of steel fibers significantly improved the crack resistance of the intelligent concrete. In the elastic stage, the resistivity of intelligent concrete of multi-scale conductive materials decreases with the increase in compression, and the decrease range of resistivity is approximately proportional to the external force. After reaching the peak load, the resistivity of the intelligent concrete gradually increases and can illustrate the damage evolution. This study lays a foundation for the application of intelligent concrete in deformation and damage monitoring.

Keywords: intelligent concrete, piezoresistivity, graphene, conductive materials, carbon black, steel fiber

OPEN ACCESS

Edited by:
Konstantin Sobolev,
University of Wisconsin–Milwaukee, United States

Reviewed by:
Ru Mu,
Hebei University of Technology, China
Marina Kozhukhova,
University of Wisconsin–Milwaukee, United States
Behrouz Farahi,
University of Wisconsin–Milwaukee, United States, in collaboration with reviewer MK

***Correspondence:**
Qiong Liu
lq@tongji.edu.cn

Specialty section:
This article was submitted to Structural Materials, a section of the journal Frontiers in Materials

Received: *12 January 2021*
Accepted: *20 May 2021*
Published: *13 September 2021*

Citation:
Wang S, Singh A and Liu Q (2021) Experimental Study on the Piezoresistivity of Concrete Containing Steel Fibers, Carbon Black, and Graphene. Front. Mater. 8:652614. doi: 10.3389/fmats.2021.652614

INTRODUCTION

Concrete is a widely used material in infrastructures for its high compressive strength and decent durability. In the past century, concrete is the most popular construction material in the world. To reduce the risk of failure and to improve the safety of the structures made with concrete, structural health monitoring (SHM) is becoming increasingly necessary, especially in some critical parts of the structures. Until now, traditional sensors, such as resistance strain gauges, piezoresistive ceramics, and optical fibers sensors, have been successfully used in SHM (Chung, 2002; Han et al., 2011). However, these kinds of sensors always have problems in durability and compatibility with concrete. To solve this, intrinsic self-sensing concrete (ISSC) was invented and has garnered increasing interest because it has similar durability to concrete and can work harmonically with normal concrete (Sobolev and Ferrada-Gutierrez, 2005; Han et al., 2015).

The self-sensing property, which was also named "piezoresistivity," of cementitious materials was first investigated by incorporating carbon fibers in concrete (Chen and Chung, 1993; Fu and Chung, 1996). Some other functional fillers were also selected to study the piezoresistivity of concrete, such as

carbon black, carbon nanotubes (CNTs), metal powder, and metal fibers, and the results showed that the resistance drops as the compressive strain increases (Li et al., 2006; HanYu and Han, 2008; Yu and Kwon, 2009). When the stress employed on intelligent concrete was greater than its elastic capacity, the resistivity would have a nonlinear raise resulting from the appearance and growth of micro-cracks and micro-damages (Chu and Chen, 2016).

The conductive filler commonly used by researchers can be roughly divided into three types, namely, fibers (carbon fibers, steel fibers, and carbon nanotubes), powder (carbon black and metal powder), and sheets (graphene and exfoliated graphite) (Blecha, 2016; Chen and Chung, 1995; Azhari and Banthia, 2012; Teomete and Kocyigit, 2013; Yoo et al., 2018). The intelligent cementitious materials containing them have different pressure sensitivity and mechanisms. Conductive fibers can not only make the cement-based materials have great pressure-sensitive characteristics but also improve the crack resistance. Particularly, the addition of a smaller amount of fibers can produce similar conductivity of concrete to powder and sheet fillers, which may result from the fact that the fibers' large length-to-diameter ratio leads to easily forming conductive pathways (Zhang et al., 2000; Lu et al., 2006; Han et al., 2009). The powder conductive filler plays a main role of micro-filling, and it was reported that the size of the powder particles and the content affect the sensitivity of the related intelligent concrete. Moreover, the intelligent concrete containing conductive powder has more stable piezoresistivity (Wang et al., 2009; Han et al., 2010; Han et al., 2011; Tang et al., 2019). In recent years, graphene, as a representative of the sheet conductive filler, has also attracted increasing interest of researchers. Because the graphene particles have a nano-scale thickness and micro-scale planar size, graphene's hybrid mechanism is similar to that of both powder and fibers at different scale levels (Kim et al., 2011; Le et al., 2014; Oskouyi et al., 2014; Liu et al., 2016; Liu et al., 2018).

Based on recent studies, valuable achievements in intelligent concrete filled with various kinds of conductive fillers are used in detecting strain and damage. When different sizes and types of conductive fillers are used together, the conductive properties and pressure-sensitive characteristics of the intelligent concrete are not clear. In this study, the intelligent concrete filled with the steel fiber, carbon black, and graphene was investigated to determine piezoresistive responses during a cyclic compressive loading, and then a compression until failure. The full strain–stress curves of concrete under compressive load can also illustrate the damage evolution process. By studying the complete damage evolution process of ISSC, suggestions for detecting the degree of damage in concrete can be provided.

MATERIALS AND TESTING METHOD

Material Preparation

The cement used in this study was standard P.O. 42.5 from Hailuo Ltd. conforming with the Chinese standard (GB175-2007, 2007). The river sand (0.0075–5 mm) and natural granite coarse aggregates (5–10 mm) were washed to remove silt content. This was done in order to remove the dust from coarse and fine aggregates because the dust particles may influence the hydration products. Normal tap water was used for mixing concrete.

Three different sizes of conductive materials were prepared to improve the piezoresistivity and mechanical properties of the intelligent concrete. The graphene obtained from Jicang Nano Tech Ltd. (Nanjing, China) was used as conductive nanoparticles. Carbon black was also adopted, which is one kind of superconductive acetylene carbon powder produced by DENKA, Japan. Copper-coated steel fibers were selected due to great durability.

The fundamental properties of graphene are listed in **Table 1**, according to which the average thickness and diameter of the graphene nano-platelets used are 2–3 nm and 5–15 μm, respectively. To facilitate the dispersion of graphene in an aqueous suspension, a polycarboxylate superplasticizer bought from Subote (Nanjing, China) was selected.

To obtain the micro-morphology of graphene, a Hitachi S-4800 field emission scanning electron microscope (SEM) was used. First, with the assistance of superplasticizer and ultrasonic water bath, graphene was dispersed in water. Then, one drop of graphene suspension was placed on an aluminum sheet. After the water evaporates, a thin graphene film was left. The aluminum sheet carrying the graphene was placed in the chamber of the SEM to capture images. The acceleration voltage is 30 kV, and the resolution can reach 10 nm. According to the SEM images, see **Figure 1**, the graphene particles show a layered and wrinkled appearance and their in-plane diameter and thickness are consistent with those reported in **Table 1**.

The images of carbon black and steel fibers under an optical microscope are shown in **Figures 2A,B**, and the size and morphology are consistent with the manufacturer's reports, which are also shown in **Table 1**.

Casting and Curing of Specimens

Graphene has a very high surface area; therefore, it requires ultrasonic treatment and the assistance of superplasticizer to disperse it in water. The graphene aqueous suspension was treated with ultrasonic waves for half an hour before being added into the mixer, as shown in the first step in **Figure 3**. The coarse aggregate, sand, carbon black, steel fibers, and cement were mixed in a planetary mixer for 30 s, as illustrated in the second step in **Figure 3**. While the mixer was running, the premixed graphene aqueous suspension was added into the mix. After 3 min of thorough mixing, the fresh concrete was ready to be cast in molds with the dimensions of 40 × 40 × 160 mm, in which two copper probes at a distance of 100 mm were pre-placed. The probe was fabricated by using the copper wires (diameter = 1 mm). The fresh concrete was filled into the molds and then compacted using a vibrating table. The specimens were demolded 24 h after casting and then stored in a standard curing room with a constant temperature of 20°C and humidity of 98%. The whole preparation procedure is shown in **Figure 3**.

The mix proportions of the intelligent concrete and contrast normal concrete are shown in **Table 2**, according to which the water/cement ratio is 0.665. For the contrast group, which is named "Con" in **Table 2**, there are no conductive materials or

TABLE 1 | Physical properties of conductive materials used in the test.

Materials	Size	Density (kg/m^3)	Specific surface area (m^2/g)	Appearance
Graphene	In-plane diameter: 5–15 μm; thickness: 2–3 nm	1,400	190	Dark powder
Carbon black	Particle diameter: ~0.045 mm	2,280	—	Dark powder
Steel fiber	Diameter: 0.2 mm; length: 10 mm	7,800	—	Copper coating

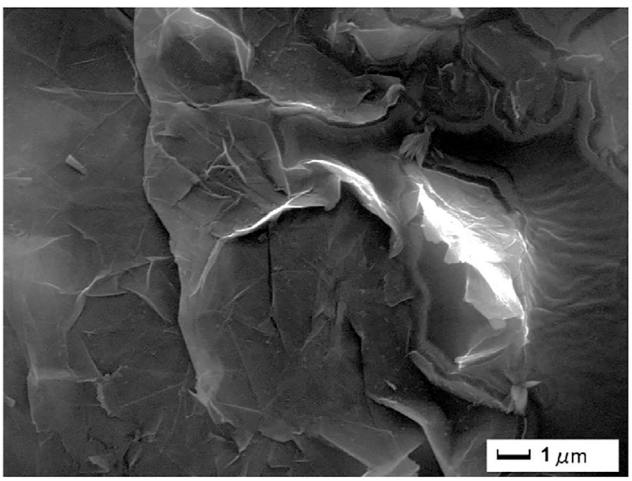

FIGURE 1 | SEM image of graphene.

superplasticizer used in the mix. In **Table 2**, the mix proportion is defined in kg/m^3. The density of the contrast concrete is 2,400 kg/m^3. The intelligent concrete was produced by adding extra conductive materials. For the intelligent concrete containing multi-scale conductive materials, which is named "M," the content of graphene is 3% of the cement by weight. The content of carbon black is 1.5% of the volume of concrete, and the content of steel fibers is 0.6% of the volume of concrete. For comparison, group G was prepared by adopting graphene alone as the conductive filler, and the graphene content is 6% of the cement by weight. According to previous studies, the intelligent concrete incorporating graphene by 6% of the cement weight was endowed with stable piezoresistivity (Liu et al., 2016).

Loading Procedure

This experiment was performed on a universal testing machine (SANS100) with a capacity of 100 kN. For applying even compressive load, the specimens were preloaded to 30% of the estimated peak load three times. After that, a cyclic load was applied on the specimen. The cyclic load started to increase from 0 to 2 kN; then, it dropped to 1 kN, increased to 4 kN, and went down to 1 kN again. The force went up to different levels, including 6 kN, 8 kN, and 10 kN, and it went back to 1 kN after reaching each level. The ultimate force of the specimens was supposed to be 30 kN. Therefore, 10 kN was applied to ensure the specimens are still within the elastic range. Polytetrafluoroethylene (PTFE) sheets that were settled on the top and bottom surfaces of the specimen were used to dismiss the friction between the platens and the specimen.

In order to obtain full stress–strain curves, a hybrid loading procedure containing a force-control phase (10 kN/min) and a displacement-control phase (0.1 mm/min) was adopted. The force-control loading was applied within 70% compressive capacity, which was estimated with the samples' mix proportion. After that, the displacement-control loading was used until the test was completed. An extensometer fixed on the backside (as to probes) of the samples was used to measure the strain. The loading setup is shown in **Figure 4**.

Measurement of Electrical Resistivity

After 28 days of curing, the specimens were stored at room temperature for one day to dry the surface. Then, they were treated by wrapping the ends with copper foil; as a result, the two ends of the specimens can be used as electrodes. The four-electrode method was selected to measure the electrical resistance of the specimens.

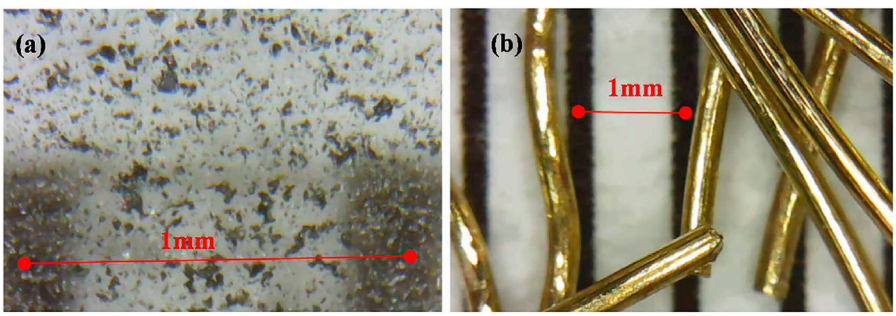

FIGURE 2 | Optical microscopic images: **(A)** carbon black; **(B)** steel fibers.

FIGURE 3 | Specimen preparation procedure.

TABLE 2 | Mix proportions.

Name	Cement	Fine aggregates	Coarse aggregates	Water	Graphene	Carbon black	Steel fiber	Superplasticizer
Con	277.0	830.9	1,107.9	184.2	0	0	0	0
M	277.0	830.9	1,107.9	184.2	8.3	34.2	46.8	8.3
G	277.0	830.9	1,107.9	184.2	16.6	0	0	16.6

Note: The unit of the mix proportion is kg/m^3.

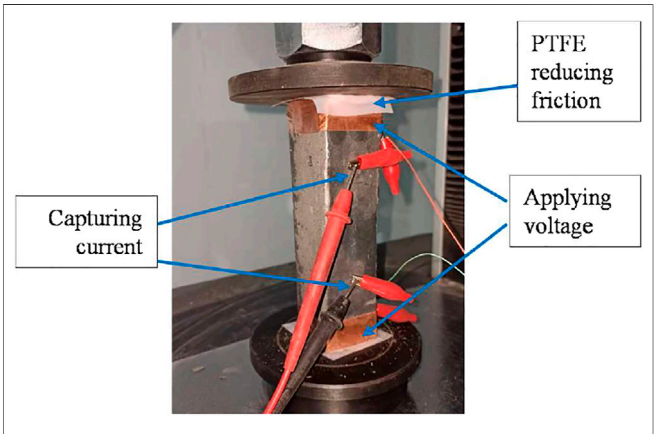

FIGURE 4 | Loading and measurement setup.

The electrical resistance was recorded while applying a uniaxial compressive load. It was measured with a four-probe method to dismiss the contact resistance between electrodes and concrete. The outer two electrodes were used for applying a constant electrical voltage of 1 V, and the inner two probes were used for the current measurement. The electrical current was captured with a universal meter (Fluke 17B). The electrical resistance can be gained by dividing the constant voltage by the captured current. Then, the resistivity ρ is calculated with the following equation:

$$\rho = VA/IL, \tag{1}$$

where V is the constant voltage, A is the area of the cross section, I is the captured electrical current, and L is the distance between the two inner probes.

TABLE 3 | Mechanical properties and resistivity.

Name	Compressive strength (MPa)	Resistivity (Ωm)	Failure modes
Con	23.4	10^6	Brittle cracks
M	25.1	0.94	Ductile cracks
G	21.1	0.90	Brittle cracks

RESULTS AND DISCUSSION

Mechanical Properties

The strength, resistivity, and failure mode of the three groups of specimens are shown in **Table 3**. It can be seen that the strength of

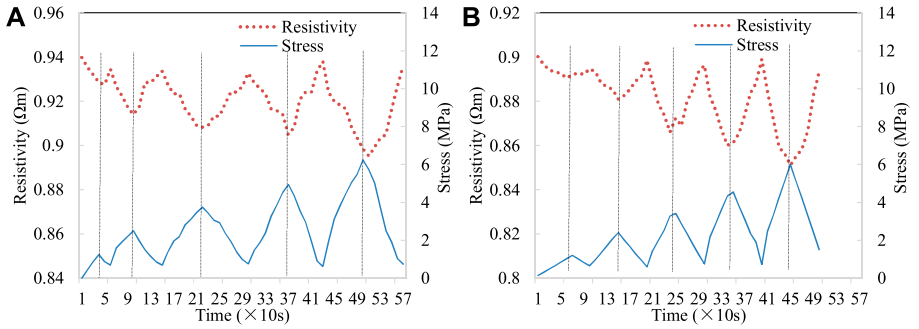

FIGURE 5 | Resistivity and loading curves during cyclic force: **(A)** group M; **(B)** group G.

group M is higher than the strength of the contrast group, 23.4 MPa. However, the strength of group G only incorporating graphene is lower. This may be because a large amount of superplasticizer is added for dispersing graphene and the superplasticizer has also a certain air-entraining effect (Liu et al., 2016). Therefore, there are more bubbles in group G intelligent concrete; as a result, the strength is weakened. Group M contains steel fibers, which restrain the propagation of cracks. This improves the strength of group M and improves its ductility more obviously. The resistivity of group M is similar to that of group G. They are 0.940 Ωm and 0.900 Ωm, respectively.

According to the above analysis, it can be found that the resistivity of groups M and G is similar. And group M has a higher strength and better ductility. In addition, the cost of group M is also lower. The amount of graphene in group M is 3% of the weight of cement, while that in group G is 6%. Considering the expensive price of graphene, the cost of group M is lower than that of group G.

Cyclic Loading

When the specimens of group M and group G are subjected to a cyclic load within the elastic stage, the resistivity of the intelligent concrete also changes cyclically, as shown in **Figure 5**. As the load increases, the resistivity decreases, and the reduction in load leads to an increasing resistivity. The amplitude change of the resistivity is roughly consistent with the force. From **Figure 5A**, it can be seen that when the load is 0kN, the resistivity of group M is 0.940 Ωm. The peak values of each cyclic load are 2 kN, 4 kN, 6 kN, 8 kN, and 10 kN, respectively. The axial compressive stress of the specimen is calculated as 1.25 MPa, 2.5 MPa, 3.75 MPa, 5 MPa, and 6.25 MPa, and the corresponding resistivity of group M is 0.929 Ωm, 0.914 Ωm, 0.908 Ωm, 0.905 Ωm, and 0.898 Ωm, respectively, which shows a downward trend. According to the difference, it can be seen that the resistivity of the intelligent concrete is approximately proportional to its axial pressure. Also from **Figure 5**, it is seen that when the load returns back to 1 kN, the resistivity of the intelligent concrete is 0.935 Ωm, 0.934Ωm, 0.932 Ωm, and 0.938 Ωm, respectively. This shows that the resistivity of the intelligent concrete in this study has a great performance of repeatability. Group G has a very similar trend of resistivity when a cyclic load is applied, see **Figure 5B**.

The linearity of a sensor is an essential property to define the degree to which the actual output curve of the sensor resembles the expected linear plot. To see the linearity of the piezoresistivity of the intelligent concrete, **Figure 6** shows the relation between the stress and the resistance captured during testing and also illustrates the best-fitting straight line and its equation. The fitting equation for group M is shown in **Figure 6A** as follows:

$$r = 0.94 - 0.0076s, \tag{2}$$

where r is the resistivity and s is the applied stress on the specimen.

The fitting equation for group G is shown in **Figure 6B** as follows:

$$r = 0.90 - 0.0087s. \tag{3}$$

The coefficient of determination (R^2) is used to evaluate the feasibility of the prediction equation as reported above. Its formula is shown as follows:

$$R^2 = 1 - \frac{\sum_i (r_i - f_i)^2}{\sum_i (r_i - \overline{r})^2}, \tag{4}$$

where r_i is the resistivity measured, $\overline{r}_i$ is the average resistivity, and f_i is the prediction result. The coefficient of determination between the fitting curve and the captured values can be calculated according to the above formula. For groups M and G, the coefficient is 0.79 and 0.95, respectively. This illustrates that the piezoresistivity of the intelligent concrete group G has a great linear relationship with the fitting function that can predict the stress performance. However, group M has an acceptable linear relationship with the fitting curve.

Failure Loading

After cyclic loading, a uniaxial compression until failure was applied on the specimen, and the resistivity recorded is shown in **Figure 7**. For group M, see **Figure 7A**, it can be seen that the resistivity continues to decline during the increased loading process. When the stress reaches the peak value of 25.1 MPa, the resistivity of the intelligent concrete decreases to the minimum value of 0.808 Ωm. After the peak, with the gradual development of cracks, the load on the specimen drops and the resistivity of the specimen increases

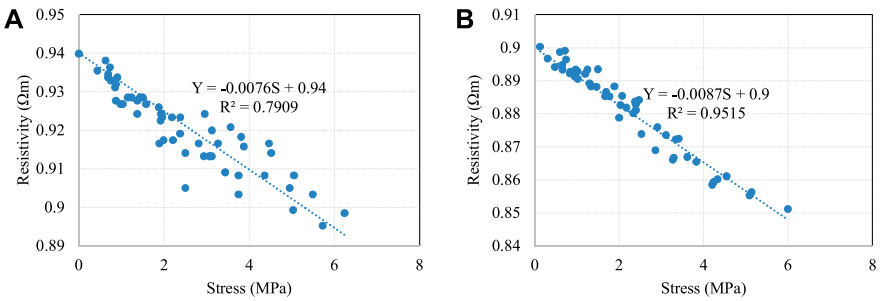

FIGURE 6 | Fitting curve and linearity: **(A)** group M; **(B)** group G.

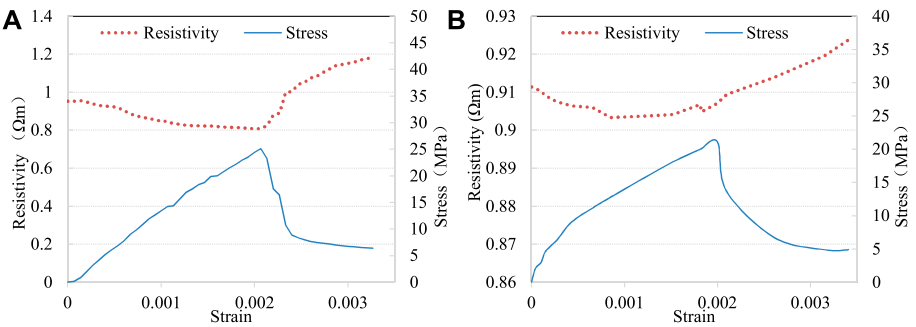

FIGURE 7 | Resistivity and loading curves until failure: **(A)** group M; **(B)** group G.

gradually. Because of the steel fibers presented, the specimen shows ductile failure and the stress–strain curve shows a relatively complete declining section. When the stress of the specimen decreases to 7 MPa, the resistivity increases to 1.139 Ωm.

The resistivity of group G also has a trend of first decreasing and then increasing as illustrated in **Figure 7B**. However, the lowest point is at about 40% of the peak load, which is the end of the elastic regime for concrete.

Damage Analysis

The damage of concrete is defined according to the effective area and the initial area of the material as follows (Mazars and Pijaudier-Cabot, 1989):

$$D = 1 - A/A_0, \tag{5}$$

where A is the effective area and A_0 is the initial area.

As the concrete damage develops, consequently, the secant modulus of it degrades. The damage of concrete is defined with the degradation of secant modulus (Chaboche, 1981; Lemaitre, 1985), as follows:

$$D = 1 - E/E_0, \tag{6}$$

where E is the present secant modulus and E_0 is the initial secant modulus. It is adopted to calculate the damage evolution curves as shown in **Figure 8**, along with strain–stress curves for comparison.

According to the classical definition of damage in **Eq. 5**, as the effective area decreases, the concrete damage develops from 0 to 1 until the concrete cannot withstand external forces. In this study, a constant voltage is applied on the intelligent concrete; therefore, the electrical current through the concrete drops with the decrease in the effective concrete area. Therefore, the damage can be defined as a function of the current as follows:

$$D = 1 - I^2/I_0^2, \tag{7}$$

where I represents the real-time current and I_0 is the initial current.

Before the peak stress, the electrical current through the intelligent concrete increases gradually, which leads to a negative damage calculated with **Eq. 7**. This is because the conductive particles in the intelligent concrete are getting close to each other under pressure. Therefore, the resistivity decreases and the current increases (Chen and Liu, 2008). But the negative damage is not meaningful for the definition of damage. Because of this, this study does not consider the descending stage of the resistivity curve to calculate the damage. As a result, the highest electrical current is regarded as the initial current.

Based on the classical damage definition, different calculating methods are proposed. In this paper, the damage evolution curves obtained with the strain–stress relationship and the electrical current passing the concrete are plotted in **Figure 8**. In **Figure 8A**, two curves of damage evolution are drawn in the same coordination, and the strain–stress curve is also provided for

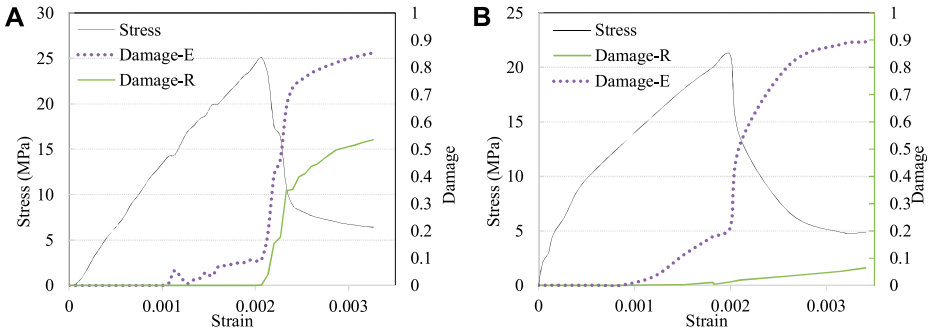

FIGURE 8 | Damage propagation: **(A)** group M; **(B)** group G.

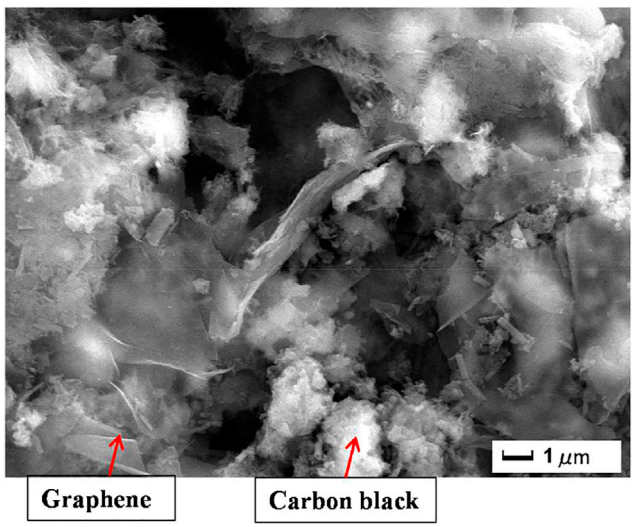

FIGURE 9 | SEM image of the microstructure of smart concrete.

comparison. It can be seen from the figure that the damage calculated with the secant modulus is zero in the elastic stage and then accumulates. The damage climbs to 0.1 at peak load and then increases rapidly to 0.7at the concave of the descending section of the stress–strain curve. After that, the damage continuously increases to 0.85, slowly.

The damage calculated with the electrical current through the specimen of group M is negative before the peak load. It increases gradually after the peak load with a small amplitude and similar trend to the damage curve calculated with secant modulus. Finally, the damage obtained with the current is about 0.32. The damage calculated with the current through the specimen is relatively small, which may result from the fact that the current can still pass through the specimen even if the specimen has splitting cracks or inclined cracks under pressure and gradually loses its bearing capacity. Although the damage characterized with the current has a disadvantage as illustrated above, it still has an obvious advantage. The current-increasing process means the stage before the peak load, and the current-decreasing process is the stage after the peak load.

For group G, the damage calculated with the secant modulus is showing a great damage evolution regular pattern, see **Figure 8B**. However, the damage determined with the resistivity has only a very small amplitude from 0 to 0.03. This may be because the failure of group G occurs between the first electrode and the second one rather than between the two inner probes, which was observed during testing.

Microstructure

The intelligent concrete is observed under the scanning electron microscope, as shown in **Figure 9**. It can be seen from the figure that the graphene is folded and flaky, which is distributed in the hardened cement paste. Carbon black can also be found in the hardened paste. The graphene nano-sheets and carbon black particles form a conductive network. Under pressure, the tunnel effect among graphene nano-sheets and carbon black can form pressure-sensitive characteristics, so as to make the concrete have intelligent performance, which can be used for strain detection and damage identification of concrete. The size of steel fibers is much larger than the scope shown in the figure, which is mainly used to prevent the brittle failure of intelligent concrete.

DISCUSSION

Three types of conductive materials are applied to the concrete, and their sizes are in millimeters, microns, and nanometers, respectively. The smallest material is nano-scale graphene, which has the same size as cement hydration products. Cement hydration products can expand by bonding to graphene (Lv et al., 2016). Carbon black of micron grade can fill the pores of cement hydration products. Appropriate doses of carbon black will not only boost the conductivity of concrete but also enhance its mechanical properties. It is apparent that the steel fibers of millimeter size will improve the crack resistance of the concrete.

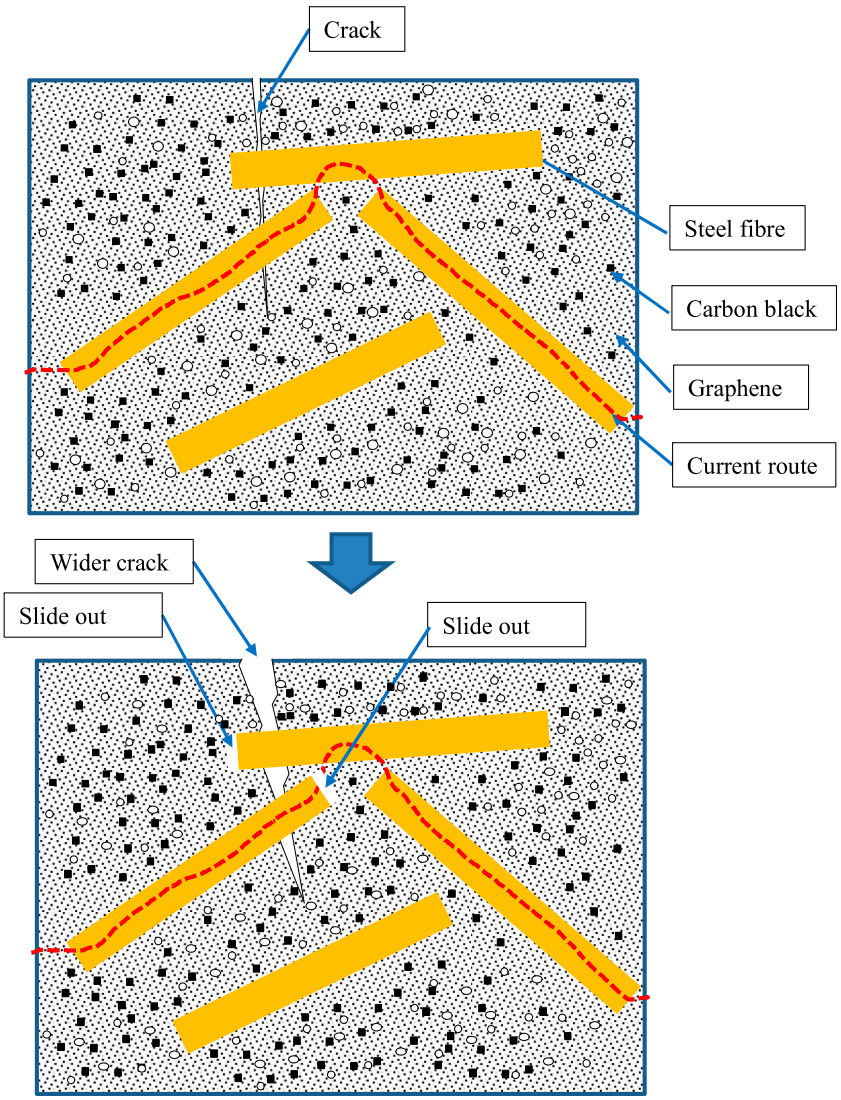

FIGURE 10 | Schematic diagram of smart concrete when cracking.

In summary, together with the characteristics of the three scales of conductive materials, the electrical conductivity of the intelligent concrete can be illustrated in this analysis by the schematic diagram shown in **Figure 10**. The yellow bars represent steel fibers, the black dots are carbon black, and graphene is scattered in the specimen. Additionally, some micro-pores also scatter in the model, which can also be found in the SEM image. The micro-pores play a role in the mechanism of contacting conduction for piezoresistivity (Han et al., 2015). As the load rises to a certain value, micro-cracks occur in the concrete. However, the presence of steel fibers not only restricts the creation of cracks in concrete but also constitutes a circuit route to ensure that the conductivity of concrete does not reduce when there are minor cracks. Only when the crack is wide enough and the steel fibers slide, will the conductive pathways be cut off and the resistance rise. This varies from the pressure-sensitive characteristics of smart concrete containing graphene alone. As graphene is applied on its own, the resistance of the associated intelligent concrete decreases in the elastic regime, which is less than 40% of the peak load. Then, the resistivity reduces with an increase in compressive load due to the creation of micro-cracks in concrete (Liu et al., 2019).

The intelligent concrete incorporating multi-scale conductive materials in this study has a special piezoresistivity such that the resistance decreases before the peak load and rises after the peak load. This property provides SHM with a desirable system. It is promising to use the positive or negative association between resistance and load to determine whether the concrete material is before or after the peak load value. If the sensor intensity ratios are organized in the framework concrete, some of them are stronger than those of the structural concrete and some of them are less strong. The structural health condition can be determined on

the basis of the test findings, and whether the concrete structure is still safe or not, and the degree of safety.

CONCLUSION

The intelligent concrete containing multi-scale conductive materials was studied in this investigation, based upon the piezoresistivity during cyclic loading and failure loading, and the following conclusions were drawn:

1) Within the elastic regime of the intelligent concrete, as the load increases, the resistivity goes down. And the resistivity climbs up when the load decreases.
2) During cyclic loading, the resistivity captured has a great linear relationship with the fitting curve, which can be used to predict the stress situation of the concrete according to piezoresistivity. The linear correlation coefficient was calculated according to the fitting formula as 0.97.
3) The resistivity continues to decline during the load-increasing process. When the stress reaches the peak at 25.1 MPa, the resistivity of the intelligent concrete decreases to the minimum value of 0.808 Ωm. After the peak, the resistivity of the specimen increases gradually with the development of cracks.
4) The damage defined with the electrical current through the intelligent concrete can illustrate the damage propagation after the peak load. Although it develops more slowly as to the damage calculated with the secant modulus, it has an advantage to show the stress and health condition of the concrete.
5) More investigations can be conducted in the future for monitoring structural health by using the intelligent concrete studied in this paper. Some sensors have strength higher than the structural concrete, and some have strength lower than structure members. The health situation can be judged according to the resistivity of the intelligent sensors and its changing trend.

DATA AVAILABILITY STATEMENT

The raw data supporting the conclusions of this article will be made available by the authors, without undue reservation.

AUTHOR CONTRIBUTIONS

SW and QL proposed the work, performed materials characterizations, and wrote the manuscript. AS revised the manuscript.

FUNDING

This work was financially supported by the Gansu Province Youth Science Foundation (20JR5RA079) Research Project of State Grid Gansu Electric Power Corporation (52273019000B).

REFERENCES

Azhari, F., and Banthia, N. (2012). Cement-based Sensors with Carbon Fibers and Carbon Nanotubes for Piezoresistive Sensing. *Cement and Concrete Composites* 34 (7), 866–873. doi:10.1016/j.cemconcomp.2012.04.007

Blecha, T. (2016). Non-destructive Detection Methods for Discontinuities of Interconnection Structures. *Microelectron. Int.* 33 (1), 23–35. doi:10.1108/mi-09-2014-0040

Chaboche, J.-L. (1981). Continuous Damage Mechanics - A Tool to Describe Phenomena before Crack Initiation. *Nucl. Eng. Des.* 64, 233–247. doi:10.1016/0029-5493(81)90007-8

Chen, P.-W., and Chung, D. D. L. (1993). Carbon Fiber Reinforced concrete for Smart Structures Capable of Non-destructive Flaw Detection. *Smart Mater. Struct.* 2, 22–30. doi:10.1088/0964-1726/2/1/004

Chen, P.-W., and Chung, D. D. L. (1995). Improving the Electrical Conductivity of Composites Comprised of Short Conducting Fibers in a Nonconducting Matrix: The Addition of a Nonconducting Particulate Filler. *Jem* 24 (1), 47–51. doi:10.1007/bf02659726

Chen, B., and Liu, J. (2008). Damage in Carbon Fiber-Reinforced concrete, Monitored by Both Electrical Resistance Measurement and Acoustic Emission Analysis. *Constr. Build. Mater.* 22 (11), 2196–2201. doi:10.1016/j.conbuildmat.2007.08.004

Chu, H.-y., and Chen, J.-k. (2016). The Experimental Study on the Correlation of Resistivity and Damage for Conductive Concrete. *Cem. Concr. Compos.* 67, 12–19. doi:10.1016/j.cemconcomp.2015.12.005

Chung, D. D. L. (2002). Electrical Conduction Behavior of Cement-Matrix Composites. *J. Mater. Eng. Perform.* 11 (2), 194–204. doi:10.1361/105994902770344268

Fu, X., and Chung, D. D. L. (1996). Self-monitoring of Fatigue Damage in Carbon Fiber Reinforced Cement. *Cem. Concr. Res.* 26, 15–20. doi:10.1016/0008-8846(95)00184-0

GB175-2007 (2007). *Common portland Cement*. Beijing, China: China National Standards Committee.

Han, B., Han, B., and Yu, X. (2009). Experimental Study on the Contribution of the Quantum Tunneling Effect to the Improvement of the Conductivity and Piezoresistivity of a Nickel Powder Filled Cement-Based Composite. *Intell. Mater. Struct.* 18 (6), 065007. doi:10.1088/0964-1726/18/6/065007

Han, B., Han, B., and Yu, X. (2010). Effects of the Content Level and Particle Size of Nickel Powder on the Piezoresistivity of Cement-Based Composites/sensors. *Intell. Mater. Struct.* 19 (6), 065012. doi:10.1088/0964-1726/19/6/065012

Han, B., Yu, X., and Ou, J. (2011). "Multifunctional and Smart Carbon Nanotube Reinforced Cement-Based Materials," in *Nanotechnology in Civil Infrastructure*. Berlin/Heidelberg: Springer, 1–47. doi:10.1007/978-3-642-16657-0_1

Han, B., Ding, S., and Yu, X. (2015). Intrinsic Self-Sensing concrete and Structures: A Review. *Measurement* 59 (1), 110–128. doi:10.1016/j.measurement.2014.09.048

HanYu, B. G. Y., Yu, Y., Han, B. Z., and Ou, J. P. (2008). Development of a Wireless Stress/strain Measurement System Integrated with Pressure-Sensitive Nickel Powder-Filled Cement-Based Sensors. *Sens. Actuators A: Phys.* 147, 536–543. doi:10.1016/j.sna.2008.06.021

Kim, Y.-J., Cha, J. Y., Ham, H., Huh, H., So, D.-S., and Kang, I. (2011). Preparation of Piezoresistive Nano Smart Hybrid Material Based on Graphene. *Curr. Appl. Phys.* 11 (1), S350–S352. doi:10.1016/j.cap.2010.11.022

Le, J.-L., Du, H., and Pang, S. D. (2014). Use of 2D Graphene Nanoplatelets (GNP) in Cement Composites for Structural Health Evaluation. *Composites B: Eng.* 67, 555–563. doi:10.1016/j.compositesb.2014.08.005

Lemaitre, J. (1985). A Continuous Damage Mechanics Model for Ductile Fracture. *J. Eng. Mater. Tech.* 107, 83–89. doi:10.1115/1.3225775

Li, H., Xiao, H.-g., and Ou, J.-p. (2006). Effect of Compressive Strain on Electrical Resistivity of Carbon Black-Filled Cement-Based Composites. *Cem. Concr. Compos.* 28, 824–828. doi:10.1016/j.cemconcomp.2006.05.004

Liu, Q., Xu, Q., Yu, Q., Gao, R., and Tong, T. (2016). Experimental Investigation on Mechanical and Piezoresistive Properties of Cementitious Materials Containing Graphene and Graphene Oxide Nanoplatelets. *Constr. Build. Mater.* 127, 565–576. doi:10.1016/j.conbuildmat.2016.10.024

Liu, Q., Gao, R., Tam, V. W. Y., Li, W., and Xiao, J. (2018). Strain Monitoring for a Bending concrete Beam by Using Piezoresistive Cement-Based Sensors. *Constr. Build. Mater.* 167, 565–576. doi:10.1016/j.conbuildmat.2018.02.048

Liu, Q., Wu, W., Xiao, J., Tian, Y., Chen, J., and Singh, A. (2019). Correlation between Damage Evolution and Resistivity Reaction of concrete In-Filled with Graphene Nanoplatelets. *Constr. Build. Mater.* 208, 482–491. doi:10.1016/j.conbuildmat.2019.03.036

Lu, J., Chen, X., Lu, W., and Chen, G. (2006). The Piezoresistive Behaviors of Polyethylene/foliated Graphite Nanocomposites. *Eur. Polym. J.* 42 (5), 1015–1021. doi:10.1016/j.eurpolymj.2005.11.026

Lv, S., Yang, W., Zhao, H., Zhou, Q., and Cui, Y. (2016). Effect of Polyacrylate/GO Nanocomposites on Properties of Cement Paste. *Mag. Concrete Res.* 68, 187–196. doi:10.1680/macr.15.00090

Mazars, J., and Pijaudier-Cabot, G. (1989). Continuum Damage Theory-Application to Concrete. *J. Eng. Mech.* 115, 345–365. doi:10.1061/(asce)0733-9399(1989)115:2(345)

Oskouyi, A., Sundararaj, U., and Mertiny, P. (2014). Tunneling Conductivity and Piezoresistivity of Composites Containing Randomly Dispersed Conductive Nano-Platelets. *Materials* 7 (4), 2501–2521. doi:10.3390/ma7042501

Sobolev, K., and Ferrada-Gutierrez, M. (2005). How Nanotechnology Can Change the concrete World: Part I. *Am. Ceram. Soc. Bull.* 84, 14–17.

Tang, Z., Li, W., Hu, Y., Zhou, J. L., and Tam, V. W. Y. (2019). Review on Designs and Properties of Multifunctional Alkali-Activated Materials (AAMs). *Constr. Build. Mater.* 200, 474–489. doi:10.1016/j.conbuildmat.2018.12.157

Teomete, E., and Kocyigit, O. I. (2013). Tensile Strain Sensitivity of Steel Fiber Reinforced Cement Matrix Composites Tested by Split Tensile Test. *Constr Build Mater.* 47, 962–968. doi:10.1016/j.conbuildmat.2013.05.095

Wang, L., Ding, T., and Wang, P. (2009). Influence of Carbon Black Concentration on Piezoresistivity for Carbon-Black-Filled Silicone Rubber Composite. *Carbon* 47 (14), 3151–3157. doi:10.1016/j.carbon.2009.06.050

Yoo, D.-Y., Kim, S., and Lee, S. H. (2018). Self-sensing Capability of Ultra-high-performance concrete Containing Steel Fibers and Carbon Nanotubes under Tension. *Sensors Actuators A: Phys.* 276, 125–136. doi:10.1016/j.sna.2018.04.009

Yu, X., and Kwon, E. (2009). A Carbon Nanotube/Cement Composite with Piezoresistive Properties. *Intell. Mater. Struct.* 18, 1–5. doi:10.1088/0964-1726/18/5/055010

Zhang, X.-W., Pan, Y., Zheng, Q., and Yi, X.-S. (2000). Time Dependence of Piezoresistance for the Conductor-Filled Polymer Composites. *J. Polym. Sci. B Polym. Phys.* 38 (21), 2739–2749. doi:10.1002/1099-0488(20001101)38:21<2739::aid-polb40>3.0.co;2-o

Conflict of Interest: SW was employed by Economic and Technical Research Institute of Gansu Electric Power Corp.

The remaining authors declare that the research was conducted in the absence of any commercial or financial relationships that could be construed as a potential conflict of interest.

Publisher's Note: All claims expressed in this article are solely those of the authors and do not necessarily represent those of their affiliated organizations, or those of the publisher, the editors and the reviewers. Any product that may be evaluated in this article, or claim that may be made by its manufacturer, is not guaranteed or endorsed by the publisher.